

## Electron paramagnetic resonance on iron-related centers in silicon

Sara H. Muller, Gijs M. Tuynman, Eric G. Sieverts, and C. A. J. Ammerlaan  
*Natuurkundig Laboratorium der Universiteit van Amsterdam, Valckenierstraat 65,  
 1018 XE Amsterdam, The Netherlands*

(Received 27 July 1981)

The behavior of interstitial iron in high-resistivity dislocation-free silicon has been studied by annealing and by electron irradiation and subsequent annealing. Annealing of iron-doped samples at temperatures above 120°C yielded one, new electron paramagnetic resonance (EPR) spectrum labeled Si-NL22. For the corresponding center we suggest a cluster of four iron atoms in a trigonal arrangement. Irradiation at about 20°C yielded many new EPR spectra, part of which are related with iron. One center with only one iron atom in trigonal symmetry was identified. Its spectrum is labeled Si-NL19. As a model we propose a  $\langle 111 \rangle$ -distorted substitutional iron atom. Four centers involving two equivalent iron atoms are formed. The spectra and tentative models are Si-NL20  $\triangleq (2\text{Fe}_i + V)^-$ , Si-NL21  $\triangleq (2\text{Fe}_i + 2V)^{+/-}$ , Si-NL24  $\triangleq (2\text{Fe}_i)^+$ , and Si-NL25  $\triangleq (2\text{Fe}_i + V)^+$ . Many spectra without resolved hyperfine interactions with iron were observed. Only one of these spectra was analyzed. This spectrum, labeled Si-NL23, has only triclinic symmetry. The formation of iron-iron pairs and the disappearance of isolated interstitial iron during irradiation at only 20°C shows that iron is subject to radiation-induced diffusion. From our study we conclude that in the absence of dislocations or acceptors as precipitation centers, isolated interstitial iron does not become substitutional during annealing. Instead it forms pairs and eventually larger clusters.

## I. INTRODUCTION

Iron is a fast-diffusing element in silicon. The diffusion coefficient at 1200°C is about  $7 \times 10^{-6}$  cm<sup>2</sup>/sec; at 900°C it is still  $10^{-6}$  cm<sup>2</sup>/sec (Ref. 1). Because of this very high diffusion coefficient, it is difficult to prevent iron contamination during heat treatment at high temperatures.<sup>2,3</sup> The solubility as a function of temperature is given by Weber and Riotte<sup>4</sup>; at 1200°C it is about  $1.5 \times 10^{16}$  cm<sup>-3</sup>, at 900°C it is only  $3 \times 10^{13}$  cm<sup>-3</sup>.

The preferential position of iron is the tetrahedral interstitial site. This follows from the high diffusion coefficient, from results of a simultaneous neutron activation analysis and EPR experiment<sup>4</sup> and from the electronic model of Ludwig and Woodbury for substitutional and interstitial transition-metal impurities in silicon.<sup>5,6</sup> By quenching from high temperatures to room temperature, the iron can almost be immobilized in the interstitial site in concentrations up to about  $1.5 \times 10^{16}$  cm<sup>-3</sup>.

Interstitial iron, Fe<sub>i</sub>, has a donor level in the band gap at  $E_v + 0.4$  eV (Refs. 7,8). Fe<sub>i</sub><sup>0</sup> and Fe<sub>i</sub><sup>+</sup> are paramagnetic. Fe<sub>i</sub><sup>0</sup> has an effective spin  $S=1$ , a  $g$  value  $g=2.070$ , and a hyperfine splitting with

<sup>57</sup>Fe of 20.94 MHz. Fe<sub>i</sub><sup>+</sup> can be described with an effective spin  $S = \frac{1}{2}$ ,  $g = 3.524$ , and a hyperfine splitting of 8.949 MHz (Ref. 9). In low-resistivity  $p$ -type material no resonance of Fe<sub>i</sub><sup>+</sup> is observed. Probably Fe<sub>i</sub> is in the doubly-positive charge state, although no EPR resonance which can be associated with Fe<sub>i</sub><sup>2+</sup> is observed.

After slow cooling from high temperatures, no isolated interstitial iron is present. The concentration of interstitial iron decreases after long storage at room temperature or after annealing at 120–170°C with an activation energy 0.7–0.8 eV (Refs. 10 and 11). The mechanism of the annealing is not yet completely understood. The various possibilities which have been suggested are the deposition on dislocations,<sup>2,11</sup> the conversion to substitutional iron,<sup>12</sup> the formation of iron-acceptor pairs,<sup>13</sup> and the clustering of iron (this paper). EPR measurements confirm the existence of iron-acceptor pairs. Ludwig and Woodbury<sup>5</sup> identified the iron-boron, iron-gallium, and iron-indium pairs. Recently also the iron-gold pair was observed in EPR.<sup>14–16</sup> Resistivity and Hall measurements show the appearance of several levels upon the annealing of the  $E_v + 0.4$  eV level, mostly one at  $E_c - 0.55$  eV (Refs. 17 and 18). A review is

TABLE I. Spin Hamiltonians and parameters of the spectra NL19—NL25. ( $D$ ,  $E$ ,  $a$ ,  $F$ ,  $T$ , and  $G$  in GHz,  $A$  in MHz).

NL19	Symmetry trigonal $g_{\perp}=2.1163\pm 0.0010$ $g_{\parallel}=2.0935\pm 0.0010$ $D=-7.84\pm 0.03$ GHz	$S=\frac{3}{2}$	$\mathcal{H}=\mu_B\vec{B}\cdot\vec{g}\cdot\vec{S}+\vec{S}\cdot\vec{D}\cdot\vec{S}+\vec{S}\cdot\vec{A}\cdot\vec{I}-\mu_N\vec{B}\cdot\vec{g}_N\cdot\vec{I}$ $A(^{57}\text{Fe})$ $A_{\parallel}=-16.0\pm 0.1$ MHz $A_{\perp}=\pm 14.7\pm 0.5$ MHz	$g_N(^{57}\text{Fe})$ $g_{N_{\parallel}}=0.18$ $g_{N_{\perp}}=\mp 0.35\pm 0.05$	
NL20	Symmetry trigonal	$S=\frac{1}{2}$ $S=\frac{5}{2}$	$\mathcal{H}_1=\mu_B\vec{B}\cdot\vec{g}\cdot\vec{S}+\sum_i(\vec{S}\cdot\vec{A}_i\cdot\vec{I}_i-g_N\mu_N\vec{B}\cdot\vec{I}_i)$ , $i$ sum over $^{57}\text{Fe}$ and $^{29}\text{Si}$ nuclei $\mathcal{H}_5=\mathcal{H}_1+\vec{S}\cdot\vec{D}\cdot\vec{S}$ , $D\gg v$ , no fourth-order terms are required $g_N(^{57}\text{Fe})\equiv 0.18$ , $g_N(^{29}\text{Si})\equiv -1.11$		
	$g_{\parallel}$	$g_{\perp}$	$A_{\parallel} (^{57}\text{Fe})$	$A_{\perp} (^{57}\text{Fe})$	
$S=\frac{1}{2}$	$2.059\pm 0.010$	$6.235\pm 0.015$	$14.4\pm 0.3$ MHz	$24.7\pm 0.8$ MHz	
$S=\frac{5}{2}$	$2.059\pm 0.010$	$2.078\pm 0.005$	$14.4\pm 0.3$ MHz	$8.2\pm 0.3$ MHz	
NL21	Symmetry monoclinic I		$S=\frac{1}{2}$ $S=\frac{5}{2}$	$\mathcal{H}=\mu_B\vec{B}\cdot\vec{g}\cdot\vec{S}-\mu_N g_N\vec{B}\cdot\vec{I}+\vec{S}\cdot\vec{A}\cdot\vec{I}$ $g_N\equiv 0.18$ $\mathcal{H}=\mu_B\vec{B}\cdot\vec{g}\cdot\vec{S}-\mu_N g_N\vec{B}\cdot\vec{I}+\vec{S}\cdot\vec{A}\cdot\vec{I}+\vec{S}\cdot\vec{D}\cdot\vec{S}$ , no fourth-order terms	$\vec{A}$ , $\vec{A}_2\parallel[0\bar{1}1]$ $\theta_A=\angle(A_1,[011])$ $A_1=9.1\pm 1.0$ MHz $A_2=26.4\pm 1.0$ MHz $A_3=37.1\pm 1.0$ MHz $\theta_A=35^\circ\pm 2^\circ$
$S=\frac{1}{2}$	$\vec{g}$ , $\vec{g}_2\parallel[0\bar{1}1]$ $\theta_g=\angle(\vec{g}_1,[011])$	$\vec{D}$ , $\vec{D}_2\parallel[0\bar{1}1]$ $\theta_D=\angle(D_1,[011])$			$A_1=9.1\pm 1.0$ MHz $A_2=26.4\pm 1.0$ MHz $A_3=37.1\pm 1.0$ MHz $\theta_A=35^\circ\pm 2^\circ$
$S=\frac{5}{2}$	$g_1=1.961\pm 0.010$ $g_2=4.90\pm 0.02$ $g_3=7.38\pm 0.03$ $\theta_g=33.8^\circ\pm 0.2^\circ$	$D_1\gg v$ $D_2=-D_1/(2.32(\pm 0.01))$ $D_3=-D_1-D_2$ $\theta_D=\theta_g$			isotropic $A=10.8\pm 1.0$ MHz
	$g_1=2.030\pm 0.010$ $g_2=2.006\pm 0.010$ $g_3=2.100\pm 0.010$ $\theta_g=33.8^\circ\pm 0.2^\circ$				

TABLE I. (Continued.)

NL22	Symmetry trigonal [A, B] <sub>+</sub> = AB + BA	S = 4	$\mathcal{H} = \mu_B \vec{B} \cdot \vec{g} \cdot \vec{S} + \vec{S} \cdot \vec{D} \cdot \vec{S} + \frac{\sqrt{2}}{36} a [S_x (S_x^3 + S_y^3 + S_z^3)]_+$ $+ \frac{1}{180} (F - a) \{ 35S_x^4 - (30S_x(S+1) - 25)S_x^2 - 6S(S+1) + 3S^2(S+1)^2 \}$ $+ \frac{1}{3040} G [ \{ 11S_x^3 - (3S(S+1) + 59)S_x \}, (S_x^3 + S_y^3) ]_+$ $F = -0.366 \pm 0.010$ GHz $G = 0.03 \pm 0.02$ GHz
NL23	Symmetry triclinic $\gamma_i$ angle between $g_i$ and its projection in the (011) plane $\delta_i$ angle between this projection and the [100] direction $g_1 = 5.489 \pm 0.01$ $g_2 = 2.809 \pm 0.01$ $g_3 = 1.768 \pm 0.01$	$S = \frac{1}{2}$ $\gamma_1 = -70.7^\circ \pm 0.3^\circ$ $\gamma_2 = 3.1^\circ \pm 0.3^\circ$ $\gamma_3 = 19.0^\circ \pm 0.3^\circ$	$\mathcal{H} = \mu_B \vec{B} \cdot \vec{g} \cdot \vec{S}$  $\delta_1 = 55.5^\circ \pm 0.4^\circ$ $\delta_2 = -25.5^\circ \pm 0.4^\circ$ $\delta_3 = 65.5^\circ \pm 0.4^\circ$
NL24 and NL25	Symmetry of the spin Hamiltonian: rhombic II $S = \frac{5}{2}$		$\mathcal{H} = \mu_B \vec{B} \cdot \vec{g} \cdot \vec{S} + \vec{S} \cdot \vec{D} \cdot \vec{S} + \frac{1}{6} a [S_x^4 + S_y^4 + S_z^4 - \frac{1}{3} S(S+1)(3S^2 + 3S - 1)]$ $+ \frac{1}{180} F \{ 35S_x^4 - [30S(S+1) - 25]S_x^2 - 6S(S+1) + 3S^2(S+1)^2 \}$ $+ \frac{1}{6} T \{ (S_x^2 + S_y^2) [9 - S(S+1) + 7S_x^2] + (S_x^2 - S_y^2) 14S_z \}$
NL24	$g_1 = 3.66 \pm 0.01$ $g_2 = 3.93 \pm 0.01$ $g_3 = 2.12 \pm 0.01$		$D_1 = E - \frac{1}{3} D$ $D = -2.32 \pm 0.02$ GHz $E = 1.00 \pm 0.03$ GHz  $a = 16.79 \pm 0.05$ GHz $F = -95.2 \pm 0.2$ GHz $T = 0.03 \pm 0.01$ GHz
NL25	$g_1 = 2.51 \pm 0.01$ $g_2 = 1.47 \pm 0.004$ $g_3 = 0.57 \pm 0.003$		$D_1 = E - \frac{1}{3} D$ $D = -2.48 \pm 0.02$ GHz $E = 2.00 \pm 0.03$ GHz  $a = -2.5 \pm 0.2$ GHz $F = -80.1 \pm 0.2$ GHz $T = 0.84 \pm 0.01$ GHz

given by Chen and Milnes.<sup>19</sup> The relation of all these levels with iron is not yet clear.

In this paper we report an EPR study of the behavior of interstitial iron in silicon. In order to study the interaction with vacancies, interstitials, and charge carriers, samples were irradiated with 1.8-MeV electrons and subsequently annealed. For comparison samples were annealed which had not been irradiated beforehand.

## II. EXPERIMENTAL PROCEDURE

In order to dope silicon with iron, samples with dimensions of  $2 \times 2 \times 20$  mm<sup>3</sup> were cleaned and covered with a solution of iron (natural or enriched to 90% <sup>57</sup>Fe) in HCl. After drying, diffusion took place at 1200°C. Half an hour is sufficient to reach the maximum concentration of natural iron.<sup>2</sup> However, to obtain an enrichment of 90% about 16 hours turned out to be necessary, probably because of the presence of natural iron contamination present in the silicon starting material. After slow cooling in order to prevent cracking, the samples are cleaned and heated again to 1200°C for about 30 minutes and quenched in water to bring the iron atoms into the interstitial position.

The concentration of iron and the enrichment with <sup>57</sup>Fe were checked with the electron spin resonance of Fe<sub>i</sub><sup>0</sup>. The angular dependence of the linewidth was used to monitor the internal stresses.<sup>20</sup> Prolonged etching between all diffusion steps and after irradiation turned out to be essential to prevent internal stresses.

Three different types of float-zone, dislocation-free, Wacker WASO silicon were used as starting materials. They will be characterized by the type (*p* or *n*), the dopant (B or P), and the resistivity in Ω cm: *p*B800, *n*P118, and *n*P8.2.

Irradiations were performed with 1.8-MeV elec-

trons from a Van de Graaff accelerator at  $290 \pm 20$  K; the dose varied between  $2 \times 10^{17}$  and  $10^{18}$  e/cm<sup>2</sup>. Via a cold tip the sample was cooled with liquid nitrogen.

EPR experiments were performed in a superheterodyne *K*-band (23 GHz) spectrometer tuned to dispersion. The spectra were observed with a modulation field of  $\sim 0.01$  mT, a modulation frequency of 80–85 Hz, and a microwave power of  $\sim 3$  μW. The scan rates varied between 0.2 and 10 mT per minute. Mostly the temperature of the sample was 1.4 K, sometimes temperatures up to 6 K were used.

## III. ANALYSIS

The observed spectra were analyzed in terms of a spin Hamiltonian. All various spin Hamiltonians are given in Table I (see also Ref. 21). Only if the spectrum could be described with an effective spin  $S = \frac{1}{2}$ , an analytical analysis was possible. In all other cases the aid of a computer was indispensable. An extensive multipurpose Fortran library (based upon the routine ZXSSQ from the Fortran library IMSL) was written by G. M. Tuynman to deal with all problems involved in the analysis of resonance spectra.<sup>22</sup> Details of the analysis will be treated separately for each spectrum.

## IV. EXPERIMENTAL RESULTS

### A. General

Upon annealing of iron-doped samples at temperatures above 120°C one, new spectrum labeled Si-NL22 is formed. Upon irradiation of iron-doped samples, many different new spectra are formed, labeled Si-NL19, NL20, NL21, NL23, NL24, and NL25. The occurrence of all these

TABLE II. Occurrence and stability of the observed spectra. ++ strong, + present, – not observed, \* produced without irradiation.

Starting material	Spectrum						
	NL19	NL20	NL21	NL22*	NL23	NL24	NL25
<i>p</i> B800	++	++	–	+	+	++	+
<i>n</i> P118	++	++	++	+	+	++	+
<i>n</i> P8.2	++	++	++	+	–	++	+
Stability (°C)±20	160	160	250	250	100	60	150
Number of iron atoms	1	2	2	–	–	2	2

spectra in different starting materials and the stability upon annealing are given in Table II. In this table the number of equivalent iron atoms as derived from the observed hyperfine interaction also can be found.

Upon irradiation and subsequent annealing, many more resonances arose. Most of them did not show resolved hyperfine interactions, but some of the weaker lines also showed a hyperfine interaction with two equivalent iron atoms. Owing to occlusion by other lines these resonances could not be analyzed. Because of the abundance of resonances we had to restrict ourselves to the analysis of interesting spectra, i.e., spectra showing hyperfine interactions or very strong spectra.

In the next sections many plots of the magnitude of the magnetic field against its direction are shown. These plots were calculated using the parameters in Table I, a microwave frequency  $\nu = 22.8722$  GHz, and a magnetic field  $\vec{B}$  in the  $(0\bar{1}1)$  plane. During the actual measurements the magnetic field was not always exactly in the  $(0\bar{1}1)$  plane due to slight misorientations of the samples. In those cases lines which are due to several otherwise equivalent orientations of the center are split, but the average position is a good approximation for the line position with  $\vec{B}$  exactly in the  $(0\bar{1}1)$  plane. The deviation of the measured or averaged position from the calculated positions (using the actual microwave frequency) was always from less than 4 mT for the anisotropic parts of the spectra to less than 1 mT for the isotropic parts. In the case of *NL19*, *NL20*, and *NL22* these errors were even less than 2 mT and 0.5 mT, respectively.

The different orientations of a  $\langle 111 \rangle$  axial center corresponding with a spectrum are labeled with the letters *a*, *b*, *c*, and *d* which denote the four  $\langle 111 \rangle$  directions:  $[\bar{1}11]$ ,  $[11\bar{1}]$ ,  $[1\bar{1}1]$ , and  $[\bar{1}\bar{1}\bar{1}]$ .

All iron-related spectra turned out to be very sensitive to internal stresses. These cause severe line broadening.

### B. Spectrum *NL19*

The angular-dependent pattern of the resonances belonging to spectrum *NL19* is shown in Fig. 1. This pattern can be analyzed with a spin  $S = \frac{3}{2}$  and the spin Hamiltonian and parameters in Table I. The sign of *D* was derived from the relative intensities of different transitions at temperatures between 1.4 and 6 K.

In Fig. 2 the line shape of transition  $2 \leftrightarrow 3$  (the

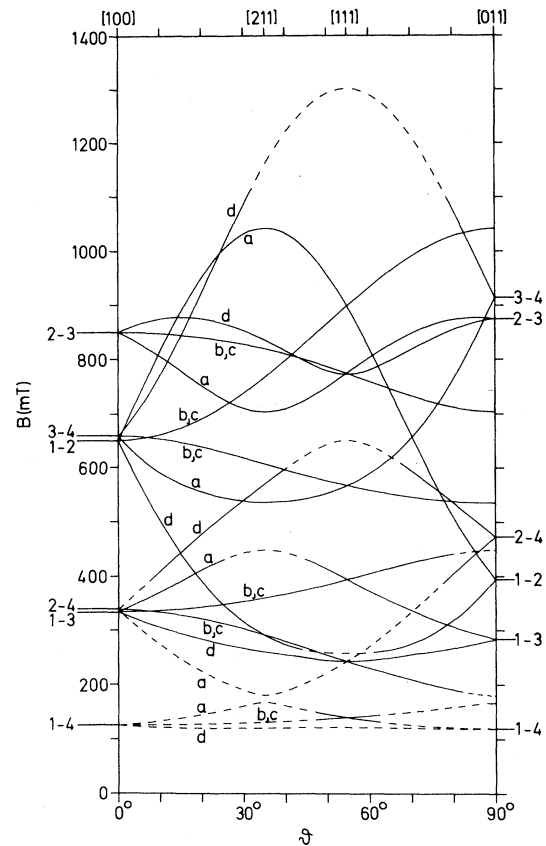


FIG. 1. Calculated angular dependence of spectrum *NL19* with  $\nu = 22.8722$  GHz. The dashed part of the pattern was not actually observed.

energy levels are numbered in order of increasing energy) is shown for some directions of the magnetic field. Only the lines of orientation *d* with  $\vec{B}$  nearly parallel to  $[111]$  and of orientation *a* with  $\vec{B}$  about  $12^\circ$  out of the  $[100]$  direction have a distinct structure [Figs. 2(a), 2(b), and 2(c)]. All other lines were broad and generally asymmetric, like the lines shown in Figs. 2(d) and 2(e). Comparison of Fig. 2(a) and Fig. 2(b), showing the same line in samples with a different  $^{57}\text{Fe}$  concentration, clearly shows the presence of one  $^{57}\text{Fe}$  nucleus. From the splitting of this line the value of  $A_{\parallel} (^{57}\text{Fe})$  was determined. The positions of the outer lines of Fig. 2(c) determine  $A_{\perp}$ . Using an isotropic nuclear *g* factor we could not explain the further hyperfine structure. The appearance of the central line in Fig. 2(c) (consisting of the two “forbidden”  $\Delta m_I = \pm 1$  transitions superposed on the resonance of 15%  $^{56}\text{Fe}$ ) determines  $g_{N_{\perp}}$ . An anisotropic nuclear *g* tensor represents a pseudonuclear Zeeman effect.<sup>23</sup> This term arises from the influ-

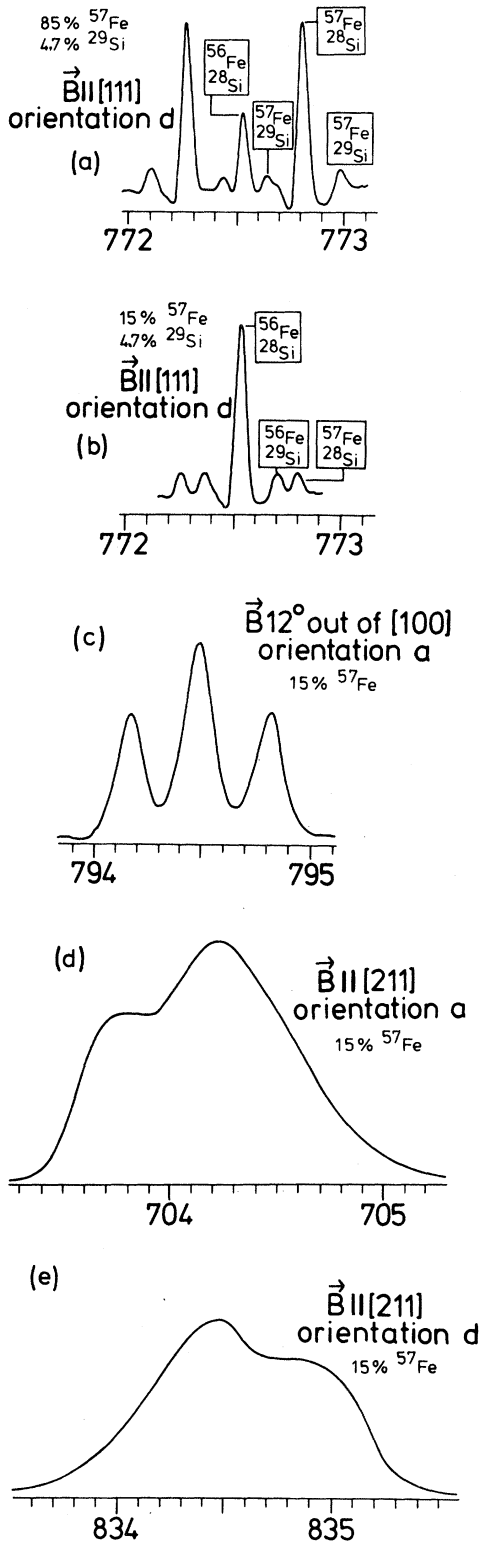


FIG. 2. Line shapes of spectrum *NL19* for various resonances of transition  $2 \leftrightarrow 3$  with  $\nu = 22.8722$  GHz and a sample temperature of 1.4 K.

ence of excited electronic states and can be derived from cross terms between the electron Zeeman interaction and the hyperfine interaction.<sup>23,24</sup> Woodbury and Ludwig<sup>25</sup> showed that for a  $\langle 111 \rangle$  axial system with  $S = \frac{3}{2}$  and a large zero-field splitting the influence of the  $m_S = \pm \frac{3}{2}$  states upon the  $m_S = \pm \frac{1}{2}$  states yields a nuclear g tensor with  $g_{N||} = g_N = 0.18$  (the normal nuclear g factor for  $^{57}\text{Fe}$ ),<sup>9</sup> while  $g_{N\perp}$  may be quite different.

The asymmetric line shape, Figs. 2(d) and 2(e), can be ascribed to an isotopic  $D$  shift.<sup>26</sup> Calculations showed that the directions and order of magnitude of the asymmetry are correct if  $D(^{56}\text{Fe})$  is about 1.0005 times  $D(^{57}\text{Fe})$ . This  $D$  shift of  $-5 \times 10^{-4}$  is large compared to the other known  $D$  shifts in silicon, found for spectrum G29 corresponding with Sn in a divacancy.<sup>26,27</sup> The  $D$  shift for this heavier atom is only  $1 \times 10^{-4}$  per unit atomic mass difference. The  $D$  shift of the six near-neighbor silicon atoms of the Sn atom is  $-0.67 \times 10^{-4}$  per unit mass. However, for a titanium-related center in  $6H\text{-SiC}$ , an even larger  $D$  shift of  $5 \times 10^{-3}$  per unit atomic mass was observed.<sup>28</sup> Because EPR spectra of *NL19* were not observable at temperatures above about 8 K, the phenomenon of the change of  $D$  with temperature, which is related with the isotope effect, could not be observed.

It is remarkable that the angular dependence of the line broadening does not show  $\langle 111 \rangle$  axial symmetry. Probably this effect is due to the influence of the internal stresses upon the linewidth. An experiment with uniaxial  $[0\bar{1}1]$  stress showed that the lines are indeed very sensitive to stress. A stress of only  $1 \text{ kg/mm}^2$  (10 MPa) already broadened the EPR lines severely. Under these circumstances most lines were broadened by about a factor of four, but for some directions and orientations the lines broadened less. In particular, the sharp lines of Fig. 2(a) broadened only 1.3 times by this external stress. The average distribution of internal stresses is not necessarily  $\langle 111 \rangle$  axial and might account for the observed angular dependence.

Altogether we can understand the line shapes of transition  $2 \leftrightarrow 3$  of spectrum *NL19* in detail with: (1) the parameters of Table I, taking into account the calculated transition probability, which is especially strongly angular dependent for the "forbidden" hyperfine transitions, (2) a zero-field splitting with a relative difference of 0.05% between  $^{56}\text{Fe}$  and  $^{57}\text{Fe}$ , and (3) a stress-induced line broadening which is not  $\langle 111 \rangle$  axial. The line shapes of those

lines of the other transitions which have some structure can be explained in the same way.

A hyperfine splitting due to three equivalent  $^{29}\text{Si}$  nuclei could only be observed with  $\vec{B} \parallel [111]$  for orientation *d* [Figs. 2(a) and 2(b)]. In all other cases the hyperfine interactions with  $^{29}\text{Si}$  were not resolved.

### C. Spectrum NL20

The calculated angular dependence of the resonances of spectrum NL20 is shown in Fig. 3. This pattern corresponding with a center with trigonal symmetry can be analyzed with an effective spin  $S = \frac{1}{2}$ , but also with a large zero-field splitting  $D$  and a half integral spin  $S > \frac{1}{2}$ .<sup>9,21,29</sup> The spin Hamiltonians and the parameters for an analysis with  $S = \frac{1}{2}$  and  $S = \frac{5}{2}$ , which yields  $g$  values close to  $g = 2$ , are given in Table I.

In this table we also find the results of the analysis of the hyperfine interactions with two equivalent iron nuclei and with one shell of silicon atoms. In Fig. 4(a) an example of a spectrum with hyperfine interactions with 85%  $^{57}\text{Fe}$  (and 4.7%  $^{29}\text{Si}$ ) is shown. The same spectrum in a sample with only the natural 2.2%  $^{57}\text{Fe}$  exhibits the  $^{29}\text{Si}$  hyperfine lines [Fig. 4(b)]. The shoulders of the central line are due to an unresolved smaller  $^{29}\text{Si}$  hyperfine interaction. These shoulders were not visible for all directions of  $\vec{B}$ . The intensity of the resolved hyperfine lines relative to the central line suggest a shell of six equivalent Si nuclei. For other directions the intensity ratio is different (sometimes a factor 2 smaller) while the lines are

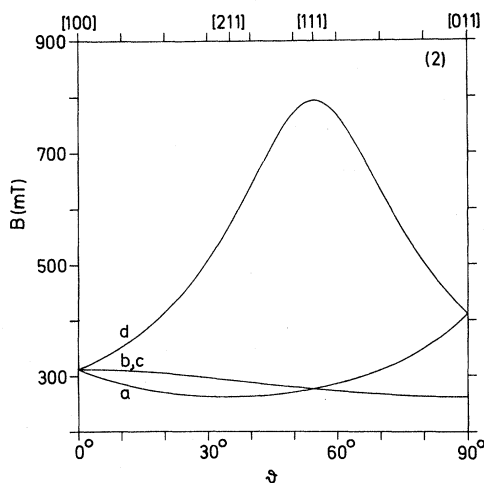


FIG. 3. Calculated angular dependence of spectrum NL20 with  $\nu = 22.8722$  GHz.

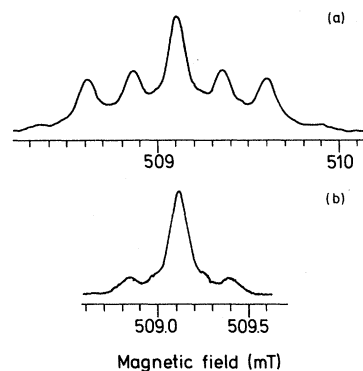


FIG. 4. Line shape of spectrum NL20 for orientation *d*, with  $\vec{B}$  in the  $(0\bar{1}1)$  plane,  $30^\circ$  out of the  $[100]$  direction,  $\nu = 22.8722$  GHz, and a sample temperature of 1.4 K. (a) 85%  $^{57}\text{Fe}$ , (b) 2.2%  $^{57}\text{Fe}$ .

broader. This can result from the lower symmetry of each of the six equivalent nuclear sites with respect to the defect. On the other hand it cannot be ruled out that the six sites are not equivalent. The resolution of the hyperfine lines was not sufficient to allow a better analysis than one with a  $\langle 111 \rangle$  axial hyperfine interaction with six nuclei.

The angular dependence of the  $^{57}\text{Fe}$  hyperfine lines relative to the central lines, as calculated with the parameters in Table I, is given in Fig. 5. The results for the two spin values differ less than the experimental uncertainties. The magnitude of  $g_N$  has only very little influence.

### D. Spectrum NL21

The calculated angular-dependent pattern of resonances given in Fig. 6 reveals monoclinic I sym-

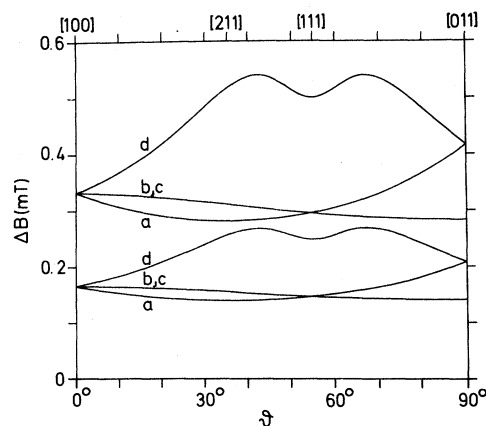


FIG. 5. Calculated angular dependence of the  $^{57}\text{Fe}$  hyperfine lines relative to the central line. The deviations from the measured splittings was less than 0.01 mT.

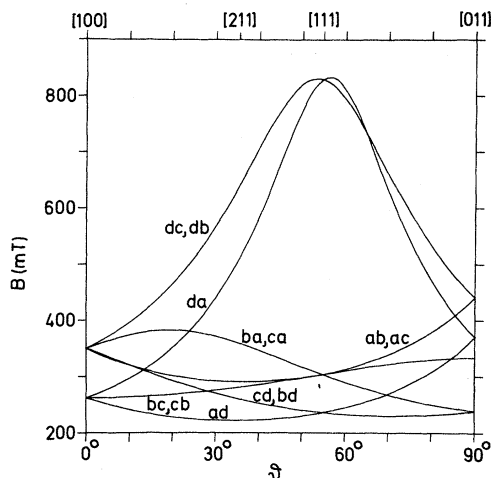


FIG. 6. Calculated angular dependence of spectrum *NL21* with  $\nu = 22.8722$  GHz.

metry. The spectrum could be analyzed with  $S = \frac{1}{2}$  (Table I). An analysis with  $S = \frac{5}{2}$ , a large zero field splitting and  $g$  values close to  $g = 2$  is also possible. However, in this case we are left with too many degrees of freedom, even if fourth-order terms are excluded, so that  $g$  and  $D$  can not be determined unambiguously. The parameters for a specific more or less arbitrary choice ( $\theta_g = \theta_D$ ) are given in Table I.

The hyperfine interaction with two equivalent  $^{57}\text{Fe}$  nuclei is shown in Fig. 7. The intensity ratio of the well-separated lines yielded a more accurate determination of the  $^{57}\text{Fe}$  enrichment than the determination from the common interstitial iron hyperfine lines which always have some overlap. The hyperfine tensor (Table I) is dependent on the choice for  $S$  and the specific restrictions on the parameters. For  $S = \frac{5}{2}$  it is not necessarily isotropic.

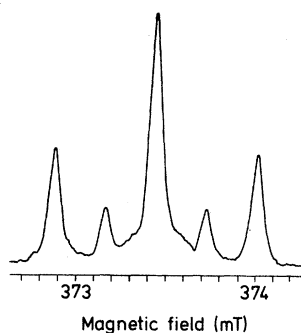


FIG. 7. Lineshape of spectrum *NL21* in a sample with 89%  $^{57}\text{Fe}$ . Spectrum for orientation *da* with  $\vec{B}$   $0.5^\circ$  out of the [100] direction in the  $(0\bar{1}1)$  plane,  $\nu = 22.8722$  GHz, and a sample temperature of 1.4 K.

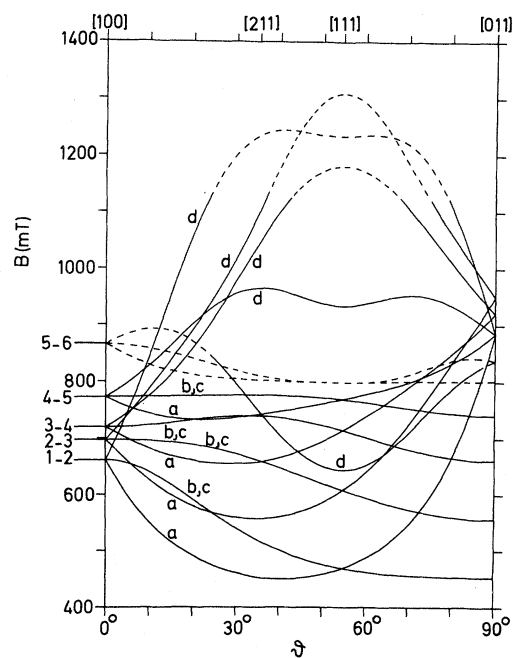


FIG. 8. Calculated angular dependence of spectrum *NL22* with  $\nu = 22.8722$  GHz. The dashed part of the pattern was not actually observed.

### E. Spectrum *NL22*

The calculated angular dependence of the observed transitions of spectrum *NL22* is shown in Fig. 8. The spectrum can be analyzed with  $S = 4$  and the spin Hamiltonian and parameters in Table I. The presence of the term with the parameter  $G$  is not very significant. Even if we do not incorporate this term in the spin Hamiltonian, the fit is nearly as good as the accuracy of the data points. More accurate measurements (more points at a slower scan rate) would give a decisive answer about the significance of this (and other) sixth-order term in the spin Hamiltonian as given by Orbach.<sup>30</sup> The relative signs of the parameters  $D$ ,  $a$ ,  $F$ , and  $G$  are determined by the angular pattern. The absolute signs were derived from the relative intensity of the different transitions at different temperatures.

Owing to the Boltzmann factor the highest energy levels, labeled 7, 8, and 9 when the levels are numbered in order of increasing energy, are hardly populated and no resonances between these levels were observed. The calculated transition probabilities for transitions  $1 \leftrightarrow 3$ ,  $2 \leftrightarrow 4$ ,  $\dots$ ,  $7 \leftrightarrow 9$ ,  $1 \leftrightarrow 4$ ,  $\dots$ , etc. turned out to be very low and we did not observe any of their resonances.

The lines of *NL22* showed no resolved hyperfine

interactions. The typical line width  $\Delta B_{1/2}$  of the various transitions was 0.7–1.0 mT, both in samples doped with  $^{56}\text{Fe}$  and with  $^{57}\text{Fe}$ .

#### F. Spectrum NL23

The complicated pattern of resonances of spectrum NL23 (Fig. 9) arises from a center with triclinic symmetry. The actual pattern was even more complicated than the calculated pattern in Fig. 9 because all lines were split into two lines due to a slight misorientation of the sample. In that case all 24 possible defect orientations give rise to separate resonances.

The spin Hamiltonian and parameters for a description with an effective spin  $S = \frac{1}{2}$  are given in Table I. Probably in this case a description with a higher spin, a large zero-field splitting, and  $g$  values close to  $g=2$  is also possible, but this was not tried.

The lines of the spectrum showed no resolved hyperfine interactions. They had a line width  $\Delta B_{1/2}$  of about 0.3 mT.

For this spectrum no model will be proposed.

#### G. Spectra NL24 and NL25

Apart from the resonances belonging to NL20 and NL21 many other lines showing a hyperfine interaction with two equivalent iron atoms were observed. These resonances showed a strong

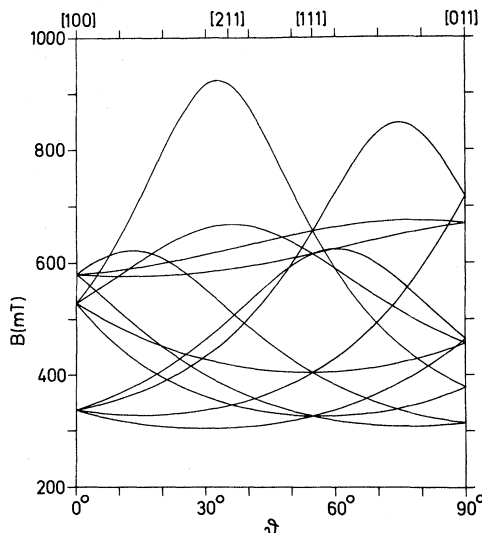


FIG. 9. Calculated angular dependence of spectrum NL23 with  $\nu = 22.8722$  GHz.

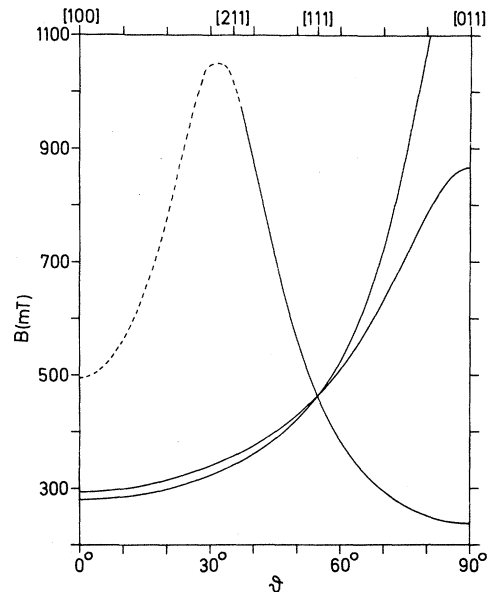


FIG. 10. Calculated angular dependence of spectrum NL24 with  $\nu = 22.8722$  GHz. The dashed part of the pattern was not actually observed.

dependence of both their intensity and their hyperfine splitting on the magnitude of the magnetic field. At high fields the lines are strong and well resolved. At low fields the lines are weak and it becomes difficult to observe their structure. The stronger spectrum NL24 nevertheless could be observed for most directions of  $\vec{B}$ , but spectrum NL25 was obscured by other spectra for directions of  $\vec{B}$  within  $50^\circ$  of the [100] direction.

It was found that the lines could be grouped with two or four lines together to form the two patterns shown in Figs. 10 and 11. The symmetry of these patterns is  $222(D_2)$ . The actual symmetry

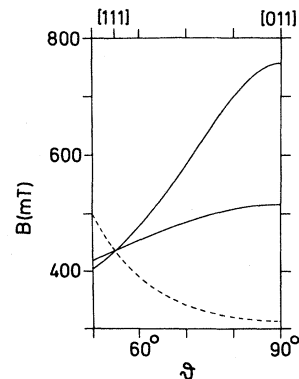


FIG. 11. Calculated angular dependence of spectrum NL25 with  $\nu = 22.8722$  GHz. The dashed part of the spectrum was not actually observed. For  $0^\circ < \theta < 50^\circ$  the spectrum was obscured by other spectra.

of the centers corresponding with *NL24* and *NL25* must be lower [probably  $2(C_2)$ ] because 222 symmetry yields only three different orientations while ten different lines were observed. Point-group symmetry 2 gives 12 different orientations of which six pairs coincide in the (011) plane. Because the deviations from 222 symmetry are only small and because we could not separate out the effect of misorientation, we only tried to analyze the average positions of the groups of lines which are close together, with a spin Hamiltonian of symmetry 222. The distance between the actually measured resonances and the average positions were up to 10 mT for both spectra.

The result of an analysis with  $S = \frac{5}{2}$  with all symmetry-allowed parameters is given in Table I. The last term in the Hamiltonian corresponds to  $T_{42} + T_{4-2}$  given by Huang *et al.*<sup>31</sup> Other fits to different data sets yielded values for the parameters which were different from the values in Table I by 10 to 50 times the given error. Nevertheless, the fits as a whole were just about as good in all measured points. This means that in fact we do not need all eight parameters but we can not make a meaningful choice among them. The deviations of the experimental data for these spectra are larger than those of *NL19* to *NL23*. Altogether, the fits of *NL24* and *NL25* are not very satisfactory. We also tried to analyze the data with different spins up to  $S = \frac{11}{2}$  but no fits were found. Besides the hyperfine interaction with  $^{57}\text{Fe}$  also hyperfine interactions with two and with eight equivalent  $^{29}\text{Si}$  nuclei were observed for *NL24*. We did not try to analyze the hyperfine tensor.

## V. DISCUSSION

### A. General

The formation of iron-iron pairs and the fast disappearance of interstitial iron during irradiation at 20°C is remarkable because noteworthy thermal diffusion of iron requires temperatures above 100°C. The observed disappearance of the  $\text{Fe}_i^0$  resonance is not due to a change of the Fermi level. Otherwise we should have observed a strong  $\text{Fe}_i^+$  resonance, which was not the case. We must therefore conclude that most iron is no longer singly interstitial after irradiation. Only part of it is traced in spectrum *NL19* and in the pair spectra *NL20*, *NL21*, *NL24*, and *NL25*. The remaining portion is incorporated in centers which are not

observed in EPR. In all, approximately a concentration of  $10^{15}$  iron pairs per  $\text{cm}^3$  is observed after an irradiation dose of  $10^{17}$  e/cm<sup>2</sup>. The concentration of nearest- and next-nearest neighbor iron pairs in a sample with a random concentration of  $1.5 \times 10^{16}$   $\text{cm}^{-3}$  is less than  $10^{11}$   $\text{cm}^{-3}$ . This means that during an irradiation of about 15 min at 20°C iron atoms must have diffused over an average of at least 150 atomic distances. Thermal diffusion over such distances requires a temperature above 120°C. Even during the irradiation the sample temperature was even locally always below 60°C, as is shown by the presence of spectrum *NL24*, which is only stable up to 60°C.

An explanation of the required diffusion distance can be found by assuming radiation-induced (or enhanced) diffusion (RID). The existence of RID has not yet been reported for iron before. For the transition metals Co, Cu, Ni, and Zn in silicon this phenomenon has been observed, however.<sup>32</sup> Our experiments are not and were not meant to be sufficient to draw any conclusions about the mechanism of the RID.

Because none of the *NL* spectra produced in irradiated material is observed in samples which were only annealed we assume that these spectra arise from centers involving one or more vacancies or silicon interstitials. For spectrum *NL24* this argument does not apply. This two-iron center, formed during the radiation-induced diffusion at 20°C, is only stable up to about 60°C. Thermal diffusion of iron, however, requires temperatures above 120°C, so that this center could not have been formed purely thermally, even if it did not contain vacancies or interstitials. We will assume that the centers involve vacancies rather than interstitials because the majority of the irradiation defects, certainly if irradiated near room temperature, involve vacancies and no interstitials.<sup>33</sup>

The production rate of the spectra *NL19*, *NL20*, and *NL24* is somewhat lower than but still comparable to the production rate of primary defects. Therefore, these centers will involve at most one vacancy. We will suggest the following models for them:  $\text{NL19} \triangleq \text{Fe}_i + V$ ,  $\text{NL20} \triangleq 2\text{Fe}_i + V$ , and  $\text{NL24} \triangleq 2\text{Fe}_i$ . Spectrum *NL21* has a lower production rate and is more stable; therefore, we assume that its center consists of two interstitial iron atoms plus two vacancies. Spectrum *NL25* also has a low production rate but its stability is comparable to the spectra *NL19* and *NL20* which involve one vacancy. Moreover the symmetry of *NL25* allows a simple split interstitial configura-

tion of two interstitial iron atoms in a vacancy. The atomic composition would then be the same as that of *NL20*, but the charge state is different, so that the position of the Fermi level will determine the intensity ratio of *NL20* and *NL25*. It is also possible that it depends on the formation process which configuration is formed. Because of the higher production rate of spectrum *NL20* this obviously will be the more likely configuration.

Spectrum *NL22* is observed in samples which are only annealed. Although we did not observe resolved hyperfine interactions, we will suggest a cluster of four interstitial iron atoms as will be outlined in Sec. V E.

Spectrum *NL23* showed no hyperfine interactions either. In that case we could only guess the atomic composition of the center and we will not present a model.

For each of the spectra the possible arrangement of the iron atoms and vacancies in the corresponding center will be discussed in the next sections. The electronic configuration and the total spin are determined similar to the way in which Ludwig and Woodbury<sup>5</sup> described transition-metal ions in silicon.

If the total spin of the center arises from spins on different atoms, these spins are coupled. In the present case it turns out that we can arrive at the observed spins if the individual spins in the center are ferromagnetically coupled.

Because all centers were observed in high-resistivity material we only consider models in which the centers are in neutral or singly positive or negative charge states.

For all described spectra the symmetry is lower than cubic so that the orbital momentum is quenched. This means that the  $g$  values must be close to the spin-only value  $g=2$ . Therefore we will prefer a description with  $S=\frac{5}{2}$  instead of  $S=\frac{1}{2}$  for the spectra *NL20* and *NL21*. The  $g$  values of spectra *NL24* and *NL25*, given in Table I, are very different from  $g=2$ . Although there was some freedom to vary the parameters without worsening the fit, as discussed in Sec. IV G, it was not possible to bring the  $g$  values close to  $g=2$ . Besides the reasons mentioned in Sec. IV G, this is another reason why we consider the analysis of *NL24* and *NL25* unsatisfactory.

### B. Spectrum *NL19*

The center corresponding with spectrum *NL19* is proposed to consist of an interstitial iron atom and

a vacancy. Probably the iron atom will form strongly-directed  $4s4p^3$  hybridized orbitals which bond with the four silicon neighbors. To arrive at  $S=\frac{3}{2}$  the total center must be positively charged. This leaves three  $3d$  electrons, with spins parallel resulting in  $S=\frac{3}{2}$ . Because the center has  $\langle 111 \rangle$  axial symmetry the iron atom can not be exactly at the substitutional position but has to be shifted along a trigonal axis, for instance, towards the tetrahedral interstitial position [Fig. 12(a)].

A distortion also follows if we apply group theory. Owing to the crystal field of the silicon lattice the energy levels of the  $d$  electrons in tetrahedral symmetry split into a doublet and a triplet. For substitutional impurity (in this case iron) the triplet state with  $d_{xy}$ ,  $d_{yz}$ , and  $d_{zx}$  orbitals has higher energy than the doublet state with  $d_{x^2-y^2}$  and  $d_{z^2}$  orbitals.<sup>5</sup> Hund's rule localizes two electrons in the  $d_{x^2-y^2}$  and  $d_{z^2}$  orbitals, and the third electron in the triplet. This gives a degenerate ground state, so that a Jahn-Teller distortion will lower the symmetry. In trigonal symmetry the triplet splits into a singlet and a doublet. Group theory yields the shape of the orbitals, giving  $(d_{xy} + d_{yz} + d_{zx})/\sqrt{3}$  for the singlet. The third electron can now be localized in this singlet orbital,

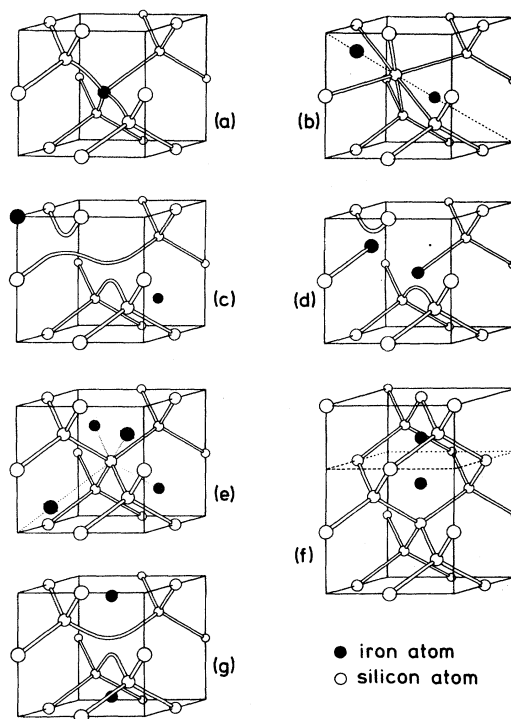


FIG. 12. Possible models for the centers corresponding with the iron-related spectra. (a) *NL19*, (b) *NL20*, (c) *NL21*, (d) *NL21*, (e) *NL22*, (f) *NL24*, (g) *NL25*.

which has the trigonal  $\langle 111 \rangle$  direction as its symmetry axis. In this way the degeneracy is lifted.

Alternative bonding configurations are also conceivable. For instance, a planar  $3d^24s$  hybridization which only binds the iron with three of the four silicon neighbors directly exhibits the  $\langle 111 \rangle$  axial symmetry. This, however, leaves a dangling bond on the fourth silicon atom. Moreover  $d^2s$  orbitals are not as strongly directed in one direction as  $sp^3$  orbitals, so that they give rise to a smaller overlap. Therefore, probably more energy will be gained by  $sp^3$  hybridization.

Hyperfine interactions with  $^{29}\text{Si}$  nuclei could only be observed with  $\vec{B} \parallel [111]$  for orientation  $d$  (see Fig. 2). The intensity of the  $^{29}\text{Si}$  hyperfine lines is consistent with the presence of three equivalent silicon atoms which can be found in the proposed model.

### C. Spectrum NL20

For the center corresponding with spectrum NL20 we propose a model of one vacancy plus two equivalent interstitial iron atoms. To arrive at the  $\langle 111 \rangle$  axial symmetry the atoms must be arranged as shown in Fig. 12(b). In that configuration the central silicon atom accepts two electrons from the iron atoms and binds by  $d^2sp^3$  hybridization<sup>34</sup> with the six neighboring silicon atoms. This shell of six equivalent nuclei is in perfect agreement with the observed intensity of the  $^{29}\text{Si}$  hyperfine interaction [see Fig. 4(b)]. Such a bonding with  $d^2sp^3$  hybridization was already proposed by Masters<sup>35</sup> for a split vacancy or semivacancy pair. It is also known from the  $\text{SiCl}_6^{2-}$  ion.

In this way the two iron atoms remain interstitial. Each of them has seven  $3d$  electrons left. If the total center is negatively charged and the iron spins are ferromagnetically coupled the total spin  $S$  equals  $\frac{5}{2}$ .

### D. Spectrum NL21

For the center corresponding with spectrum NL21 a model of two equivalent iron atoms and two vacancies is proposed. If we transfer  $3d$  electrons to  $4s4p^3$  states for bonding with the silicon atoms and between the two iron atoms, we arrive at a total spin  $S=4$  or  $S=0$  in the neutral defect for ferromagnetic and antiferromagnetic coupling,

respectively. This requires at least a threefold charge state in order to arrive at  $S=\frac{5}{2}$ . Moreover, the center would have  $\langle 111 \rangle$  axial symmetry. Therefore, a configuration as shown in Fig. 12(c) or 12(d) is more likely.

In the model of Fig. 12(c) the silicon dangling bonds pair off as in the "empty" divacancy.<sup>36</sup> The iron atoms are near their normal tetrahedral interstitial sites. Each of them has eight  $3d$  electrons. Ferromagnetic coupling and a singly positive charge state yields  $S=\frac{5}{2}$ . The long extended bond in this model is, in fact, hardly a bond. This suggests a different model, shown in Fig. 12(d).

In this model the iron atoms are situated near the substitutional sites. One  $3d$  electron of each of the iron atoms is transferred to a  $4s4p$  hybridized state to bind with one silicon atom. The four remaining silicon bonds are still mutually paired off. Each iron atom has seven  $3d$  electrons left. Ferromagnetic coupling and a singly negative charge state yield  $S=\frac{5}{2}$ .

Comparing the two models we notice two major differences: the charge state and the (non)existence of iron-silicon bonds. Because NL21 was only observed in  $n$ -type silicon a negative charge state is more likely, favoring the second model. If a direct iron-silicon bond is present we would expect resolved hyperfine interactions with  $^{29}\text{Si}$ . These were not observed (see for instance Fig. 7). This favors the first model. All together, we cannot make a meaningful choice between these two models.

### E. Spectrum NL22

The model which we suggest for spectrum NL22 is a cluster of four interstitial iron atoms. A possible  $\langle 111 \rangle$  axial arrangement is shown in Fig. 12(e), where one of the iron atoms is displaced along the axis so that it is no longer equivalent with the other three. In addition, an arrangement in which all four iron atoms are situated on a row along the  $\langle 111 \rangle$  direction is possible.

The spin  $S=4$  arises from the ferromagnetically-coupled spins of the four iron atoms with  $S=1$ . The total center is neutral, in accordance with its appearance in high ohmic materials (Table II). Spectrum NL22 is formed when the EPR spectrum of single neutral interstitial iron starts to disappear as shown in Fig. 13. If this spectrum disappears fast (above  $150^\circ\text{C}$ ) the intensity of NL22 also decreases, but it does not disappear completely.

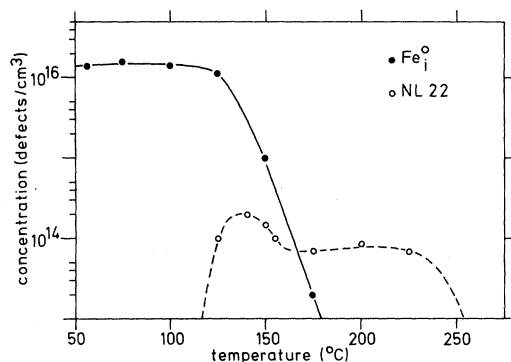


FIG. 13. Occurrence of the resonances of  $\text{Fe}_i^0$  and spectrum  $NL22$  as a function of anneal temperature. The relative accuracy of concentrations of the same center at different temperatures is about a factor 1.5, the absolute accuracy is not better than a factor ten.

Under these conditions one can think that part of the four clusters grow to larger clusters. The remaining four clusters dissociate at about  $250^\circ\text{C}$ .

It is known that another transition metal, manganese, also forms clusters of four atoms in silicon. The spectrum of this center was described by Ludwig *et al.*<sup>37</sup> Their model of a cluster with cubic symmetry was based upon the well-resolved hyperfine interactions with four equivalent manganese atoms. In our case we did not observe a resolved hyperfine interaction with iron for  $NL22$ . A possible explanation can be derived from Table III in which we compare some data on hyperfine interactions with Mn and Fe in silicon.

We note that the nuclear  $g$  factor of manganese is about ten times larger than that of iron. Assuming the same electron probability on the nucleus, this is in accordance with the observed hyperfine parameters which are also about ten times larger

for Mn. The cluster of four Mn atoms has a hyperfine parameter which is at least three times smaller than that of isolated Mn. If the same applies for iron, we expect that the hyperfine splitting of  $NL22$  is at most 0.1–0.2 mT. Because the (in)homogeneous line broadening (for instance due to random stresses) causes a linewidth of 0.7–1.0 mT (see Sec. IV E), it is not surprising that no resolved hyperfine splitting is observed.

Because the lines of  $NL22$  show no structure in EPR we cannot say anything definite about the hyperfine interaction and the configuration of the iron atoms. Electron-nuclear double resonance measurements are necessary to solve these problems.

#### F. Spectrum $NL24$

For the center corresponding with spectrum  $NL24$  we propose a model with only two interstitial iron atoms. The two iron atoms are situated on equivalent sites very close to a  $\langle 100 \rangle$  axis to give the approximate  $222$  symmetry, in the way shown in Fig. 12(f) or on both sides of the central silicon atom. In fact, the figure shows a center with  $\bar{4}2m$  ( $D_{2d}$ ) symmetry. In the similar case of a  $\langle 100 \rangle$  split silicon di-interstitial, Lee *et al.*<sup>38</sup> show which distortions of the defect lower the symmetry from  $\bar{4}2m$  to  $222(D_2)$  or even to  $2(C_2)$ . In a singly-positive charge state the center will have a spin  $\frac{5}{2}$  if the  $3d$  electrons of the iron atoms are ferromagnetically coupled.

The two iron atoms in Fig. 12(f) have ten silicon neighbors around them. In the approximation of  $222$  symmetry they can be classified in three shells of, respectively 4, 4, and 2 atoms which are equivalent by symmetry. The observed  $^{29}\text{Si}$  hyper-

TABLE III. Hyperfine interactions with Mn and Fe in silicon.

	$^{55}\text{Mn}$	$^{57}\text{Fe}$
Nuclear $g$ factor	1.4	0.18
Typical hyperfine parameter of centers with one atom	120–270 MHz <sup>a</sup>	9–21 MHz <sup>a,b,c</sup>
Hyperfine parameter of cluster of four atoms	38 MHz <sup>a</sup>	?

<sup>a</sup>G. W. Ludwig and H. H. Woodbury, *Solid State Phys.* **13**, 223 (1962).

<sup>b</sup>This work.

<sup>c</sup>R. L. Kleinhenz, Y. H. Lee, J. W. Corbett, E. G. Sieverts, S. H. Muller, and C. A. J. Amerlaan, *Phys. Status Solidi* **108**, (1) (in press).

fine lines can arise from these shells if the hyperfine interactions of the four-atom shells are accidentally degenerate.

The two iron atoms are thought to be brought together by RID during the electron irradiation. Purely thermally these pairs cannot be formed in a short time, as they are unstable at temperatures at which the iron atoms become sufficiently mobile.

### G. Spectrum NL25

For the center corresponding with spectrum NL25 we propose a model of two interstitial iron atoms and a single vacancy. The two iron atoms are situated on equivalent sites very close to a  $\langle 100 \rangle$  axis to give the approximate  $22\bar{2}$  symmetry [Fig. 12(g)]. For the exact symmetry the same applies as for spectrum NL24. The dangling bonds of the four silicon neighbors are paired off in the way as for the single negative vacancy. The spin  $S = \frac{5}{2}$  arises from the two iron atoms with  $S = 1$  and a single positive charge. This is a different atomic arrangement of the model for spectrum NL20 in a different charge state (see Secs. V A and V C).

### H. Hyperfine interactions

An analysis of the hyperfine parameters of transition metals in silicon in terms of atomic wave functions is complicated and does not lead to very satisfactory results. A common linear-combination-of-atomic-orbitals (LCAO) analysis cannot be applied to centers with a spin  $S > \frac{1}{2}$ . We can only use modified formulas<sup>39</sup>:

$$a = \frac{8}{3} \pi g \mu_B g_N \mu_N |\psi_s(0)|_{\text{eff}}^2$$

and

$$b = \frac{2}{7} g \mu_B g_N \mu_N \langle r_d^{-3} \rangle_{\text{eff}}$$

with  $a$  the isotropic and  $b$  the anisotropic (traceless) part of the hyperfine tensor.

For spectrum NL19 this analysis leads to the values  $|\psi_s(0)|_{\text{eff}}^2 = 0.7 \text{ \AA}^{-3}$  and  $\langle r_d^{-3} \rangle_{\text{eff}} = 0.6 \text{ \AA}^{-3}$ . The given model for NL19 localizes the three paramagnetic electrons in  $3d$  orbitals of the iron atom. The isotropic part then probably arises from core polarization of the  $1s$ ,  $2s$ ,  $3s$ , and  $4s$  shells. Using calculations of Watson and Freeman<sup>40</sup> we estimate for a free ion in a  $3d^3 4s$  configuration:  $|\psi_s(0)|^2 \approx 3 \text{ \AA}^{-3}$ . The one-electron values for  $\langle r_d^{-3} \rangle_{\text{eff}}$  vary between  $25 \text{ \AA}^{-3}$  for a  $3d^9$

and  $40 \text{ \AA}^{-3}$  for a  $3d^5$  configuration. If more electrons are present we must consider the total charge distribution. In some special cases (e.g., a filled shell) the resulting  $\langle r^{-3} \rangle_{\text{eff}}$  is zero,<sup>39</sup> but this is not the case in the proposed electronic arrangement of NL19.

Both  $|\Psi_s(0)|_{\text{eff}}^2$  and  $\langle r_d^{-3} \rangle_{\text{eff}}$  are small compared to the calculated values. This is not due to a considerable charge transfer to orbitals on neighboring silicon atoms. In that case large hyperfine interactions with  $^{29}\text{Si}$  should have been observed. Also for other transition metals in silicon the observed hyperfine interactions are unexpectedly small. A satisfactory explanation of this phenomenon has not yet been given, although some attempts have been made.<sup>6,41,42</sup> Recently spin-restricted scattered-wave  $X\alpha$  calculations on interstitial  $3d$  transition-metal impurities have been performed by DeLeo *et al.*<sup>6</sup> Their first results indicate that the associated levels in the band gap arise from valence band states which become localized on the impurity atom for a fair part and acquire a considerable fraction of  $d$  character. These results may very well agree with the observed reduced-wave-function parameters.

A quantitative analysis of the hyperfine interactions of the pair spectra will not be given. On the one hand these spectra have about the same hyperfine interactions with  $^{57}\text{Fe}$  and no large hyperfine interactions with  $^{29}\text{Si}$ . On the other hand the analysis will be even more complicated because the spin  $S = \frac{5}{2}$  is a result of the coupling of the spins on two atoms. Sieverts *et al.*<sup>39</sup> show the consequences of such a coupling for the analysis of the interaction in the case of the AuFe complex. In that case the interactions with gold and iron can be distinguished and the contributions of the individual spins can be sorted out. Here we will restrict ourselves to a qualitative comparison of the different hyperfine interactions. The isotropic parts of the hyperfine interactions of NL20 and NL21 are both 10 to 11 MHz. The hyperfine splitting of NL24 and NL25 was not analyzed, but corresponds probably also with a hyperfine interaction with an isotropic part of about the same magnitude. This is in accordance with the models for all these four pair spectra in which the iron atoms all have the same electron configuration.

## VI. CONCLUSIONS

Irradiation of iron-doped silicon at  $20^\circ\text{C}$  yields many new EPR spectra, part of which are related

with iron. The following tentative defect models have been proposed:  $NL19 \triangleq (Fe_i + V)^+$ ,  $NL20 \triangleq (2 Fe_i + V)^-$ ,  $NL21 \triangleq (2 Fe_i + 2V)^{+/-}$ ,  $NL24 \triangleq (2 Fe_i)^+$ , and  $NL25 \triangleq (2 Fe_i + V)^+$ . The model for  $NL19$  is in fact a  $\langle 111 \rangle$ -distorted substitutional iron atom. The models for  $NL20$  and  $NL25$  differ in their detailed configuration and in their charge state.

The formation of iron pairs and the disappearance of isolated interstitial iron during irradiation at only 20°C shows that iron is subject to radiation induced diffusion. Annealing of iron-doped samples above 120°C yields one, new spectrum,  $NL22$  for which we suggest a cluster of four interstitial iron atoms. Although no resolved iron hyperfine interactions have been observed, the observed spin, the formation kinetics, and a comparison with a  $Mn_4$  cluster strongly support this model.

Upon annealing at 25 to 200°C spectrum  $NL19$ , associated with substitutional iron, requires the presence of vacancies and does not occur spontaneously. This is a confirmation of earlier notions of the behavior of iron in silicon.<sup>4</sup>

From our results it follows that iron has a tendency to form clusters during the radiation-

induced diffusion. Under these conditions vacancies interact in the clustering process. It has already been shown before that iron forms pairs with acceptors<sup>5</sup> and with gold.<sup>14,15,16</sup> It has also been found that iron is deposited on dislocations.<sup>2,11</sup> Our experiments on high-resistivity dislocation-free silicon show that upon annealing in such materials iron most probably forms clusters.

The level in the band gap at  $E_C - 0.55$  eV which has been reported to arise upon annealing (see Sec. I) is in boron-free silicon probably associated with a cluster with some definite number of iron atoms and not with substitutional iron or a multivacancy-iron complex.<sup>19</sup>

The observed hyperfine interactions confirm that the atomic-wave-function parameters of iron in silicon are considerably reduced in comparison to free atoms or atoms in ionic crystals, as is also the case for other transition-metal ions in silicon.

#### ACKNOWLEDGMENT

This work was supported in part by the Foundation for Fundamental Research of Matter (FOM).

- 
- <sup>1</sup>J. D. Struthers, *J. Appl. Phys.* **27**, 1560 (1956).  
<sup>2</sup>E. Weber and H. G. Riotte, *Appl. Phys. Lett.* **33**, 433 (1978).  
<sup>3</sup>H. J. Rijks, J. Bloem, and L. J. Giling, *J. Appl. Phys.* **50**, 1370 (1979).  
<sup>4</sup>E. Weber and H. G. Riotte, *J. Appl. Phys.* **51**, 1484 (1980).  
<sup>5</sup>G. W. Ludwig and H. H. Woodbury, *Solid State Phys.* **13**, 223 (1962).  
<sup>6</sup>G. G. DeLeo, G. D. Watkins, and W. Beall Fowler, *Phys. Rev. B* **23**, 1851 (1981).  
<sup>7</sup>H. Feichtinger, J. Walzl, and A. Gschwandtner, *Solid State Commun.* **27**, 867 (1978).  
<sup>8</sup>J. D. Gerson, L. J. Cheng, and J. W. Corbett, *J. Appl. Phys.* **48**, 4821 (1977).  
<sup>9</sup>G. W. Ludwig and H. H. Woodbury, *Phys. Rev.* **117**, 1286 (1960).  
<sup>10</sup>Y. H. Lee, R. L. Kleinhenz, and J. W. Corbett, *Appl. Phys. Lett.* **31**, 142 (1977).  
<sup>11</sup>L. S. Milevskii, L. G. Vavarina, and N. T. Bendik, *Izv. Akad. Nauk SSSR Neorg. Mater.* **12**, 1382 (1976).  
<sup>12</sup>N. T. Bendik and L. S. Milevskii, *Dokl. Akad. Nauk SSSR* **195**, 107 (1970).  
<sup>13</sup>W. H. Shepherd and J. A. Turner, *J. Phys. Chem. Solids* **23**, 1697 (1962).  
<sup>14</sup>Y. H. Lee, R. L. Kleinhenz, and J. W. Corbett, in *Proceedings of the International Conference on Defects and Radiation Effects in Semiconductors, Nice, France, 1978*, edited by J. H. Albany (Institute of Physics, Bristol, England, 1979), Ser. **46**, p. 521.  
<sup>15</sup>M. Höhne, *Phys. Status Solidi B* **99**, 651 (1980).  
<sup>16</sup>R. L. Kleinhenz, Y. H. Lee, J. W. Corbett, E. G. Sieverts, S. H. Muller, and C. A. J. Ammerlaan, *Phys. Status Solidi* **108**, (1) (in press).  
<sup>17</sup>C. B. Collins and R. O. Carlson, *Phys. Rev.* **108**, 1409 (1957).  
<sup>18</sup>N. T. Bendik, V. S. Garnyk, and L. S. Milevskii, *Fiz. Tverd. Tela* **12**, 1693 (1970) [*Sov. Phys.—Solid State* **12**, 1340 (1970)].  
<sup>19</sup>J. W. Chen and A. G. Milnes, *Annu. Rev. Mater. Sci.* **10**, 157 (1980).  
<sup>20</sup>M. Berke, E. Weber, and H. Alexander, *Solid State Commun.* **20**, 881 (1976).  
<sup>21</sup>S. H. Muller, thesis, University of Amsterdam, 1981 (unpublished).  
<sup>22</sup>This library may be obtained by writing to Dr. C. A. J. Ammerlaan. (Payment may be required).  
<sup>23</sup>A. Abragam and B. Bleaney, *Electron Paramagnetic Resonance of Transition Ions* (Clarendon, Oxford, 1970).  
<sup>24</sup>J. M. Baker and B. Bleaney, *Proc. R. Soc. London Ser. A* **245**, 156 (1958).  
<sup>25</sup>H. H. Woodbury and G. W. Ludwig, *Phys. Rev.* **117**, 1287 (1960).  
<sup>26</sup>G. D. Watkins, *Solid State Commun.* **17**, 1205 (1975).

- <sup>27</sup>G. D. Watkins, *Phys. Rev. B* **12**, 4383 (1975).
- <sup>28</sup>K. M. Lee, Le Si Dang, and G. D. Watkins, *Solid State Commun.* **37**, 551 (1981).
- <sup>29</sup>G. E. Pake and T. L. Estle, *The Physical Principles of Paramagnetic Resonance* (Benjamin, Reading, Mass., 1973).
- <sup>30</sup>R. Orbach, *Proc. R. Soc. London Ser. A* **264**, 458 (1961).
- <sup>31</sup>Huang W. H., Lin F. C. and Zu J. K. *Proc. Phys. Soc.* **84**, 661 (1964).
- <sup>32</sup>A. J. Koifman, A. N. Narkulov, B. K. Oksengendler, and M. S. Yunusov, *Phys. Status Solidi A* **38**, 439 (1976).
- <sup>33</sup>E. G. Sieverts, thesis, University of Amsterdam, 1978 (unpublished).
- <sup>34</sup>R. McWeeny, *Coulson's Valence* (Oxford University Press, London, 1979).
- <sup>35</sup>B. J. Masters, *Solid State Commun.* **2**, 283 (1971).
- <sup>36</sup>G. D. Watkins and J. W. Corbett, *Phys. Rev.* **138**, A543 (1965).
- <sup>37</sup>G. W. Ludwig, H. H. Woodbury, and R. O. Carlson, *J. Phys. Chem. Solids* **8**, 490 (1959).
- <sup>38</sup>Y. H. Lee, N. N. Gerasimenko, and J. W. Corbett, *Phys. Rev. B* **14**, 4506 (1976), Fig. 8.
- <sup>39</sup>E. G. Sieverts, S. H. Muller, C. A. Y. Ammerlaan, R. L. Kleinhenz, and J. W. Corbett, *Phys. Status Solidi* **108**, (2) (in press).
- <sup>40</sup>R. E. Watson and A. J. Freeman, *Phys. Rev.* **123**, 2027 (1961).
- <sup>41</sup>M. Jaros, *Adv. Phys.* **29**, 409 (1980).
- <sup>42</sup>F. S. Ham and G. W. Ludwig, in *Paramagnetic Resonance*, edited by W. Low (Academic, New York, 1963), Vol. I, p. 130.